# Breast Ultrasound Tomography Versus MRI for Clinical Display of Anatomy and Tumor Rendering: Preliminary Results

Bryan Ranger[1]
Peter J. Littrup[1]
Nebojsa Duric[1]
Priti Chandiwala-Mody[2]
Cuiping Li[1]
Steven Schmidt[1]
Jessica Lupinacci[1]

**OBJECTIVE.** The objective of our study was to determine the clinical display thresholds of an ultrasound tomography prototype relative to MRI for comparable visualization of breast anatomy and tumor rendering.

**SUBJECTS AND METHODS.** Thirty-six women were imaged with MRI and our ultrasound tomography prototype. The ultrasound tomography scan generated reflection, sound-speed, and attenuation images. The reflection images were fused with the components of the sound-speed and attenuation images that achieved thresholds to represent parenchyma or solid masses using an image arithmetic process. Qualitative and quantitative comparisons of MRI and ultrasound tomography clinical images were used to identify anatomic similarities and optimized thresholds for tumor shapes and volumes.

**RESULTS.** Thresholding techniques generated ultrasound tomography images comparable to MR images for visualizing fibrous stroma, parenchyma, fatty tissues, and tumors. In 25 patients, tumors were cancerous and in 11, benign. Optimized sound-speed thresholds of 1.46 ± 0.1 and 1.52 ± 0.03 km/s were identified to best represent the extent of fibroglandular tissue and solid masses, respectively. An arithmetic combination of attenuation images using a threshold of 0.16 ± 0.04 dB/cm (mean ± SD) further characterized benign from malignant masses. No significant difference in tumor volume was noted between benign or malignant masses by ultrasound tomography or MRI ($p > 0.1$) using these universal thresholds.

**CONCLUSION.** Ultrasound tomography is able to image and render breast tissues in a manner comparable to MRI. Using universal ultrasound tomography threshold values for rendering the size and distribution of benign and malignant tissues appears feasible without IV contrast material.

**Keywords:** breast cancer, breast imaging, dynamic contrast-enhanced MRI, MRI, ultrasound tomography

DOI:10.2214/AJR.11.6910

Received March 24, 2011; accepted after revision July 20, 2011.

This work was support by a grant from the Michigan Economic Development Corporation (grant 06-1-P1-0653).

[1]Karmanos Cancer Institute, 3990 John R Rd, Harper Professional Bldg, Ste 710, Detroit, MI 48201. Address correspondence to P. J. Littrup (littrupp@karmanos.org).

[2]Wayne State University School of Medicine, Detroit, MI.

*AJR* 2012; 198:233–239

0361–803X/12/1981–233



Breast MRI has recently been elevated to the preferred screening choice for high-risk women and is recognized as an important adjunctive examination to mammography and ultrasound for the evaluation of breast tumor size and extent [1–5]. The utility of MRI in investigating breast cancer is largely because of its high sensitivity and moderate specificity for masses larger than 5 mm, including ductal carcinoma in situ (DCIS) [6, 7]. By analyzing breast morphology and enhancement characteristics, MRI uses qualitative and quantitative data about tumor vascularity to better differentiate between benign and cancerous masses [8–13]. MR scanners, however, are costly to purchase, house, and maintain and require dedicated staff for uniform operation and interpretation [14].

These disadvantages have limited the widespread use of breast MRI for diagnosis and staging and have made screening of the general population cost-prohibitive. Consequently, a modality that could cost-effectively rival MRI's overall image quality could have a broad societal impact. Breast ultrasound tomography can provide operator-independent and reproducible scanning with quantitative tissue characterization capabilities [15–26]. Ultrasound tomography can accurately portray several acoustic properties of insonified tissue including margin definition, tissue elasticity, sound speed, and attenuation [27–31] for potential improvements in clinical differentiation of benign and malignant breast masses.

As previously described in a preliminary study [20], our goal was to assess whether ultrasound tomography can generate images comparable to MRI in a reproducible manner using universal diagnostic parameters. This article presents a larger cohort of patients than

in the prior study [20] using improved image fusion methods for a novel ultrasound tomography prototype in comparison with standard breast MR images. A specific process was defined whereby an imaging sequence could routinely produce fused images of ultrasound tomography reflection, sound-speed, and attenuation data for rendering of normal architecture and tumor volumes comparable to MRI in preparation for future multicenter clinical trials and a commercial product.

## Subjects and Methods

### *Patient Selection and MR Dataset*

All ultrasound tomography imaging examinations were performed under an institutional review board–approved protocol in compliance with HIPAA with informed consent from all patients. Patients were recruited on the basis of prior ultrasound or mammography findings of focal mass effect. Each patient was scanned with our clinical ultrasound tomography prototype after mammography and standard ultrasound examinations but before ultrasound-guided biopsy, as previously described [20–26]. The population selection criteria restricted our analysis to cases for which we had both ultrasound tomography reconstructions and breast MR images obtained within 6 weeks of the ultrasound tomography examination. MRI was performed for standard clinical indications from available prior scans and was not the focus of this study other than for morphologic comparisons. Thus, the MR scanner and sequence details are beyond the scope of this study and a limited overview is provided: Unenhanced and gadolinium-enhanced MR sequences of all patients were reviewed by a board-certified radiologist with more than 15 years of experience in breast imaging and a senior radiology resident.

MR scans were received from our PACS as axially oriented images that were then reformatted using a public domain image analysis package, ImageJ [32], into coronal views to match the native format of the ultrasound tomography acquisitions. Gadolinium-enhanced fat-saturated T1-weighted images were used to define the volume and extent of all solid tumors. T2-weighted images were used to identify cysts. Our patient dataset represents an array of breast sizes, patient ages, and breast densities and contains both benign and cancerous lesions (Table 1). The disproportionate number of cancer patients ($n$ = 25) was anticipated because most breast MR scans were obtained for staging purposes.

### *Ultrasound Tomography Device and Data Acquisition*

The principles and technical details of our clinical ultrasound tomography device have been described [20–26]. In summary, the patient lies in the prone position on the examination bed with the breast suspended through a hole in a thin, pliable sail cloth opening into a water tank. This design allows immersion of the breast, including the axillary tail, into the water bath with flexible contouring to the chest wall. During the beginning phases of clinical trials the ultrasound tomography scan was limited to the coronal levels surrounding a primary mass because of limited memory storage. Hence, some secondary masses may have gone undetected because they were out of the scanning range of those particular studies.

A ring transducer, operating at a current central frequency of 1.5 MHz, encircles the breast and scans from the patient's chest wall to the nipple region by means of a motorized gantry. The 1.5-MHz frequency allows penetration across the 20-cm ring diameter, but the compound imaging from circumferential transducers and algorithms reduces speckle and clutter for better-than-anticipated contrast resolution at this frequency. The transducer consists of 256 elements that sequentially emit and receive ultrasound signals. The speed of sound in water is about 1.5 km/s, which is similar to that in breast tissue. Water serves as a coupling medium between the breast and transducer. Transmission and reflection ultrasound signals are subsequently recorded at a sampling rate of 6.25 MHz to obtain 30–115 tomographic slices of the breast (depending on the breast size) at 1-mm intervals for a scan range of 3.0–11.5 cm on this prototype. The acquisition time of a complete scan per breast is approximately 1 minute.

Three types of ultrasound tomography images of the entire coronal cross section throughout the whole breast are produced from the raw data using previously described tomographic reconstruction algorithms [21–23, 26]: reflection, sound speed, and attenuation. Reflection images, derived from changes of acoustic impedance, provide echotexture data and anatomic detail for the entire breast. Reflection images are valuable for defining tumor margins and architectural distortion that can be used to characterize lesions through the BI-RADS criteria [33]. Sound-speed images are based on the arrival times of acoustic signals. Previous studies have shown that cancerous tumors have elevated sound speed relative to normal breast tissue [29, 31], a characteristic that can aid in the differentiation of fat, normal tissue, and masses. Attenuation images are tomographic reconstructions based on acoustic wave amplitude changes. Higher scatter and greater absorption in cancers cause greater attenuation of ultrasound waves [28–30] so that attenuation data in conjunction with sound speed may provide an effective method for differentiating malignant from benign solid tumors. However, limited-angle tomography with standard linear-array transducers cannot discriminate differences in breast tissue [31].

Quantitative attenuation and sound-speed values by ultrasound tomography may help differentiate tumors in a manner similar to some BI-RADS characteristics, such as posterior shadowing (or high attenuation), that have a greater association with cancer. Similarly, high sound speed is a reflection of higher density (i.e., $c = \sqrt{K/\rho}$, where $c$ = sound speed, $K$ = bulk modulus, and ρ = density). Higher density, in turn, corresponds to potentially greater stiffness and improved cancer discrimination by elastography [34]. Therefore, artifacts of standard ultrasound are potentially quantified by ultrasound tomography (i.e., shadowing corresponding to attenuation) because circumferential imaging eliminates standard artifacts of shadowing, refractions, and so on.

### *Image Analysis*

The three types of ultrasound tomography images can be combined without geometric discrepancy by means of image fusion. A macro developed for ImageJ was used to fuse reflection ($I_r$), attenuation ($I_a$), and sound-speed ($I_s$) ultrasound tomography images and to adjust image thresholds before their combination. However, before fusion of reflection, sound speed, and attenuation can be considered, the thresholds needed to be validated according to the appropriate anatomic size representation. Coronal

**TABLE 1: Patient Characteristics ($n$ = number of patients)**

| Patient Characteristic | Value |
|---|---|
| Age (y), mean ± SD | 45.9 ± 11.6 |
| Diagnosis ($n$ = 36) | |
| Cancer (invasive ductal carcinoma) | 25 |
| Benign (cyst, fibroadenoma, fibrosis, or adenosis) | 11 |
| Breast density, ($n$ = 36) | |
| Fatty tissue (< 10%) | 2 |
| Scattered fibroglandular tissue (11–50%) | 8 |
| Heterogeneously dense fibroglandular tissue (51–75%) | 18 |
| Dense fibroglandular tissue (> 75%) | 8 |

T1 fat-saturated gadolinium-enhanced MR images were used as the gold standard by which ultrasound tomography images and associated pathologic correlations were done. Specifically, the size and extent of both normal structures (e.g., fibroglandular tissue) and masses were taken from the qualitative appearance rather than a quantitative measurement on MRI. Sound-speed and attenuation thresholds on ultrasound tomography were thus adjusted to match the appearance of fibroglandular tissues and mass sizes on MRI. Thresholds were then iteratively assessed to finalize a single threshold that could be applied to all patients.

Image fusion allows multiparameter visualization so that multiple characteristics can be viewed as one image and breast tissue features can be evaluated more efficiently and comprehensively (Fig. 1). In addition to accentuating masses, fused images depict local and surrounding tumor effects, including parenchyma and breast architecture. Parenchymal tissue was visualized by varying the rendered range of sound speeds in the ultrasound tomography images and assigning these values to gray scale to match the appearance of parenchyma in the MR images. This sound-speed threshold ($x$) was noted for each patient. Depiction of solid masses was similarly optimized using a combination of sound-speed and attenuation thresholds, applying a colored value to these pixels, and comparing the results with dynamic contrast-enhanced MRI (DCE-MRI) renderings of the same lesions at maximum enhancement. The associated sound-speed and attenuation thresholds for similar mass size and extent were noted for each patient ($y$ and $z$, respectively). A final fused image, $I_f$, was created by combining the reflection image, $I_r$, the threshold sound-speed image, $I_s$, and threshold attenuation image, $I_a$, as indicated by the following formula:

$$I_f = I_f + I_{s>x} + \left[I_{s>x} \wedge I_{a>z}\right] + \left[I_{s>x} \neg I_{a>z}\right]$$

where ^ denotes the logical AND operation; ¬ is the logical NOT operation; and $x$, $y$, $z$ are the variable threshold values defined. The final image thereby simultaneously displays overall breast architecture (via $I_r$), parenchyma (via $I_s$), and solid masses (via $I_s$ ^ $I_a$ and $I_s$ ¬ $I_a$). For image fusion, sound-speed images with total variation regularization [23] were used because of their increased ability to better define the sharpness of lesion edges and to dampen ray artifacts.

The similar resolutions of MRI and ultrasound tomography enabled an effective comparison with this fusion process. The spatial resolution of the MR data is approximately 1 mm and the image slices are typically 1 mm thick. The ultrasound tomography images are characterized by an in-plane spatial resolution of 1–2 mm with a slice thickness of approximately 4 mm. The parameters used during the comparison process were the size of the primary tumor, the presence of additional suspicious lesions, and the distribution of parenchymal and fibroglandular tissues. To compare masses rather than the overall breast architecture, we relied on the observation that masses tend to have higher sound speeds relative to background tissue. A "detected mass" by ultrasound tomography was defined as a distinct feature appearing in one or more ultrasound tomography modalities that coincided in location and size with masses identified on the corresponding MR images.

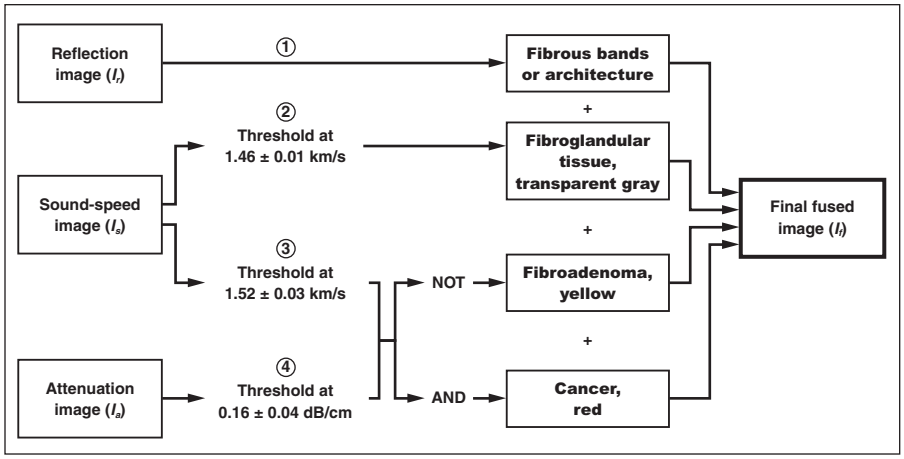


**Fig. 1**—Diagram shows fusion method. First, reflection, sound-speed, and attenuation images are obtained from ultrasound tomography scanner. Reflection image depicts fibrous architecture and is used as background. Two separate thresholds are applied to sound-speed image: 1.46 ± 0.01 km/s to show parenchyma and 1.52 ± 0.03 km/s to depict solid mass. Threshold of 0.16 ± 0.04 dB/cm and logical AND and NOT operators are then applied to attenuation image, respectively. Circled numbers represent steps in image fusion. Final fused image then shows benign solid mass as yellow or cancer as red. **Boldface** represents tissue estimates.

Once a preliminary relationship was suggested by visual assessment, a quantitative technique was used to verify that these ultrasound tomography thresholds were producing images analogous to MR images. First, we reviewed available standard ultrasound and MR studies of all patients to determine the number of masses within an approximate breast volume covered by ultrasound tomography. Ultrasound and pathology data were used to verify and correct for any obvious tumor size discrepancy by MRI because of its tendency to overestimate tumor size relative to pathologic measurements [5]. To estimate lesion volumes, we applied the ellipsoid formula ($\varpi$ / 6 × length × width × height) to tumor measurements obtained on ultrasound tomography and MRI. We also used a 3D region of interest that encompassed the mass and subsequently applied a threshold to determine the margins of the mass and its extent most similar to the MRI findings. A pixel count based on the built-in "Histogram" function of ImageJ was then used to accumulate a volume measurement.

We calculated the mean of the thresholds used in volume calculations to determine whether a unique, universally applicable threshold could be ascertained. Using these average thresholds for sound speed and attenuation, we recalculated the volumes of each mass to determine the variation of mean-threshold–acquired volumes to actual lesion volumes.

### *Statistical Analysis*

Assessment was limited to observational differences and was not intended to power the sample size of the study. All mean value comparisons for volume differences between ultrasound tomography and MRI mass volumes used the two-tailed Student $t$ test. Significance was declared at $p < 0.05$.

## Results

Adjusting thresholds in the fused images to match the tumor sizes noted on MR images, as shown in equation 1, yielded a mean value of $x$ = 1.46 ± 0.01 km/s for delineating parenchyma, and mean values of $y$ = 1.52 ± 0.03 km/s and $z$ = 0.16 ± 0.04 dB/cm to render solid masses. For solid masses, cancers were clearly differentiated and displayed as red when both thresholds were met, whereas benign masses (e.g., fibroadenomas) were yellow because they met only the sound-speed threshold. A visual assessment of the images led to the identification of parenchyma, fibrous stroma, masses, and fatty tissues on both ultrasound tomography and MR images. Components of normal breast anatomy had similar distributions on ultrasound tomography and MRI (Fig. 2) and the semitransparent lighter gray regions represented

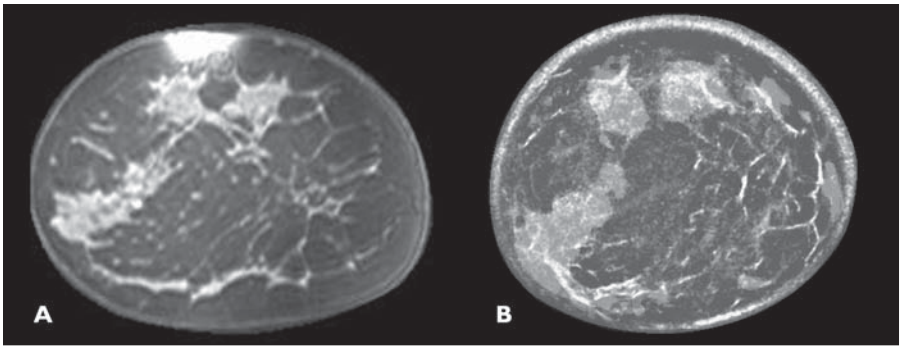


**Fig. 2**—45-year-old woman with scattered breast density.
**A** and **B,** Coronal T1 fat-saturated enhanced MR image (**A**) and fused ultrasound tomography image (**B**) show similar anatomic distribution of fibrous bands and overlying fibroglandular tissue. In **B**, dark gray corresponds to fat and semitransparent lighter gray represents denser fibroglandular tissue with underlying thin white fibrous bands.

step 2 of the fusion process, as noted in the flowchart shown in Figure 1.

Utilizing the reflection image as background in the fused image, we could identify cysts by their clearly defined smooth boundaries (Fig. 3). Other benign lesions, such as fibroadenomas, also showed smooth boundaries, but the mass content was colored yellow in fused images when the NOT operation identified that only the sound-speed threshold of 1.52 km/s was surpassed (Fig. 4). Reflection images suggested poor visualization of tumor margins for cancers (Fig. 5) in our small sample set, but the radio frequency component of the reflection image (reflection image utilizing the raw acoustic signal with no envelop fitting) [26] also showed more discernible architectural distortion of the surrounding normal tissue than nearly all MR images (Figs. 5C and 5D).

By applying our universal thresholds to the ultrasound tomography images, we found that ultrasound tomography fusion images showed masses of similar size and location to those shown on DCE-MRI (Fig. 6). Furthermore, Figure 6 emphasizes ultrasound tomography's ability to accurately image the irregular margins of an invasive carcinoma extending into parenchymal tissue without the use of contrast enhancement. Comparison of ultrasound tomography with standardized contrast-enhanced fat-saturated MR images showed that the ultrasound tomography depiction of tumor extent corresponded to mass margins identified by MRI. In all cases, ultrasound tomography detected invasive ductal carcinoma when present in the scanning range. DCIS was not part of the dataset for evaluation.

Of 36 patients with 55 masses noted on MRI, 48 masses were identified on ultrasound tomography. The seven masses that ultrasound tomography did not detect were secondary masses that were not within the scanning range for that particular study. Lesion volumes were calculated from ultrasound tomography data by dimensional analysis and by applying our universal thresholds and were then compared with similarly determined volumes from MRI. There was no significant difference between benign or malignant mass volumes by ultrasound tomography or MRI ($p > 0.05$).

## Discussion

Tumor extent by ultrasound tomography was shown prospectively to be similar to DCE-MRI when masses simultaneously exceeded thresholds of 1.52 ± 0.03 km/s for sound speed (total variation regularized) and 0.16 ± 0.04 dB/cm in attenuation. These values were attained by assessing their volumetric performance in accurately representing the distribution of benign and malignant tissues noted from MRI as the anatomic gold standard. Specifically, these thresholds allowed fibroglandular tissue and tumors to have a similar volumetric appearance as on MRI. However, ultrasound tomography thresholds for sound speed and attenuation cannot be directly compared with prior absolute literature values ob-

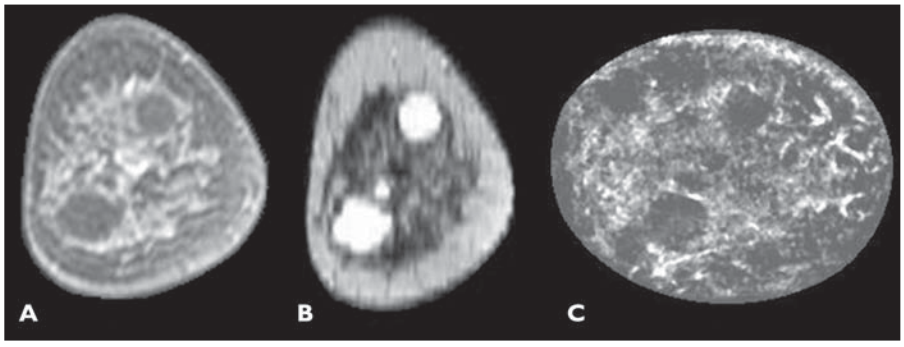


**Fig. 3**—52-year-old woman with heterogeneously dense breasts.
**A,** Two simple cysts in 1- and 7-o'clock positions are seen on coronal T1 fat-saturated enhanced MR image.
**B,** Cysts have much better contrast on this T2 image than on **A**.
**C,** Reflection ultrasound tomography image shows these simple cysts did not reach sound-speed thresholds or attenuation threshold for solid masses.

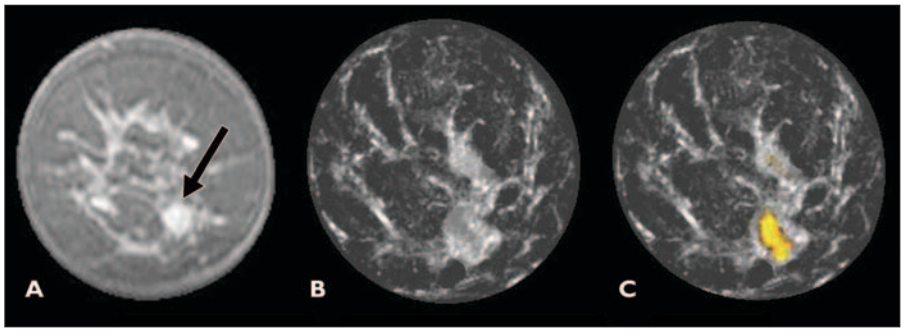


**Fig. 4**—43-year-old woman with 1-cm fibroadenoma in 5-o'clock position.
**A** and **B,** Coronal fat-saturated gadolinium-enhanced MR image (**A**) and ultrasound tomography image obtained after step 2 of fusion process (**B**) caused fibroadenoma (*arrow*, **A**) to be obscured by adjacent fibroglandular tissue because that entire region surpassed sound-speed threshold of 1.46 km/s.
**C** and **D,** Final fused ultrasound tomography image now shows benign yellow overlay color from NOT operator function, whereby sound-speed threshold of 1.52 km/s was surpassed but attenuation threshold was not surpassed.

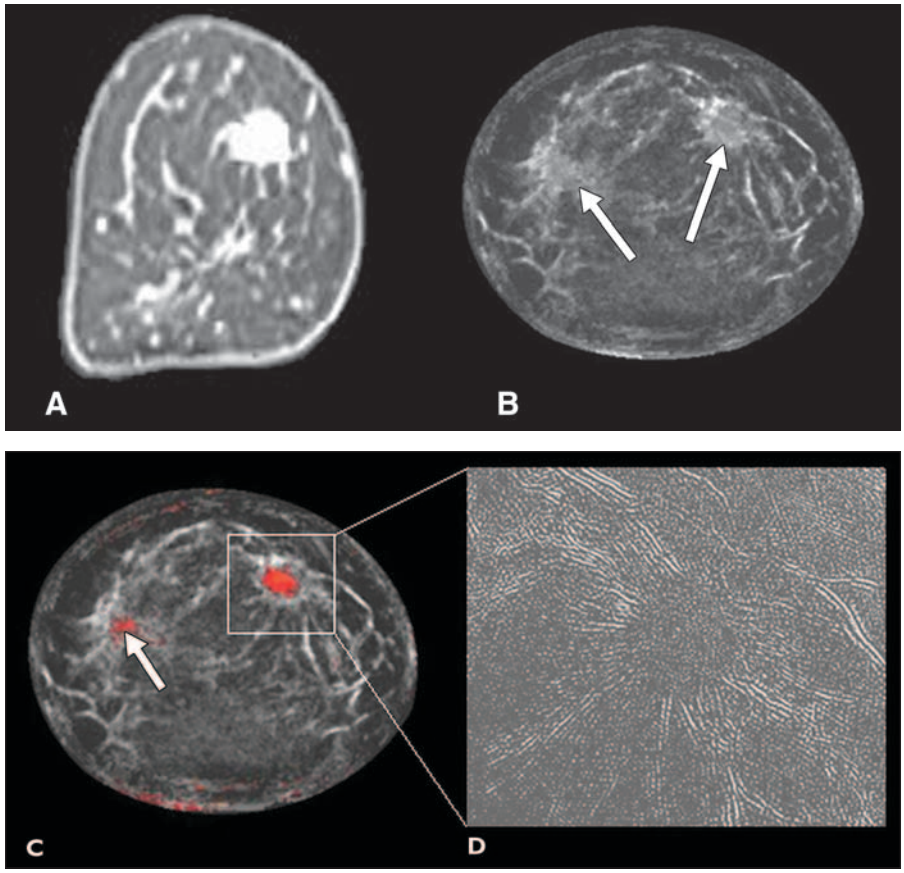


**Fig. 5**—56-year-old woman with 1.7-cm invasive ductal carcinoma in 1- to 2-o'clock position showing bright enhancement.
**A** and **B,** Coronal T1 fat-saturated enhanced MR image (**A**) and initial fused ultrasound tomography image obtained after step 2 of fusion process (**B**) only shows two semitransparent lighter gray regions (*arrows*, **B**) that achieved first fibroglandular threshold of 1.46 km/s.
**C,** Final fused ultrasound tomography image obtained usin AND operator now produces red overlay for mass in 1- to 2-o'clock position because it had both high sound speed and high attenuation, whereas only tiny regular portion of 9-o'clock region surpassed both thresholds (*arrow*). Some parenchyma and fibrous band junctions can incidentally reach threshold (9- to 10-o'clock position) but were easily excluded as not having mass effect on several slices.
**D,** Magnified reflection image using radio frequency component shows distinct mass effect with prominent architectural distortion corresponding to region around cancer seen in **C**.

tained from in vitro specimens and different ultrasound frequencies [29, 30] or from relative in vivo measurements using standard ultrasound [31]. Indeed, our presented ultrasound tomography thresholds represent the first in vivo values obtained from tissue discrimination during automated whole-breast scanning. Prior in vivo measurements by limited-angle tomography using a standard linear-array transducer obtained only relative measurements from a specified region of interest and could not discriminate attenuation differences between fat, cancer, and benign tissues [31]. Conversely, an ultrasound tomography ring array allows a full aperture for a better signal-to-noise ratio, particularly for attenuation estimates.

Although our ultrasound tomography thresholds were then prospectively used for all patients in this study, these thresholds show only the feasibility of creating a standardized imaging approach and do not reflect diagnostic values to discriminate benign from malignant tissue at this time. Such discrimination requires further evaluation of thresholds relative to surrounding normal tissue for each patient to better control for natural individual tissue variations. An evaluation of the diagnostic performance of ultrasound tomography is beyond the scope of this article and will be thoroughly addressed in an upcoming study evaluating patients undergoing breast biopsy. Again, the overall imaging rendering concept of ultrasound tomography is important to validate because technology improvements in future commercial units will further refine the absolute quantitative values and diagnostic thresholds needed for optimal tissue discrimination.

Qualitative comparison of the fused ultrasound tomography images with T1 fat-saturated gadolinium-enhanced MR images using the calculated thresholds showed similar mass contrast and overall appearance. Anatomic differences can be accounted for by dissimilar breast deformation under MRI (air) and ultrasound tomography (water) examination conditions, lower spatial resolution of ultrasound tomography images, and greater slice thickness associated with ultrasound tomography images. The concordance of breast anatomy visualized by ultrasound tomography and MRI (Fig. 3) suggests that the effect of current reconstruction artifacts and that errors associated with ultrasound tomography imaging are modest and do not limit the interpretation of ultrasound tomography images. Furthermore, current ultrasound tomography artifacts, which are primarily Nyquist frequency–based streak artifacts, will be markedly reduced as technology rapidly increases transducer number in the ring with associated improvements in reconstruction algorithms.

Benign masses tended to have properties similar to those of normal breast tissue. Consequently, their characterization relied on reflection images to detect smooth margins found with cysts (Fig. 3) and fibroadenomas. In addition to their smooth margins on reflection images, fibroadenomas could be visualized in the fused images when using the NOT operation (Fig. 4). Fibroadenomas normally exhibited higher sound speed than surrounding tissue but not much attenuation of the acoustic wave possibly because of their relatively homogeneous histology and minimal scirrhous reaction or lack of interaction with surrounding normal tissues. Conversely, cancers showed poor margin discrimination by reflection alone because of the reduced echo contrast of irregular margins due to peripheral invasion or tissue interaction. Therefore, the ability of reflection images to display architectural distortion of

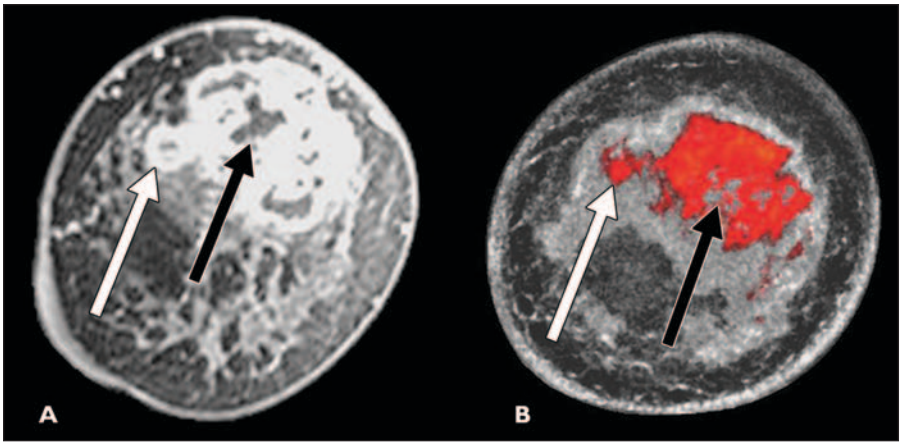


**Fig. 6**—50-year-old woman with heterogeneously dense breasts.
**A,** Coronal T1 fat-saturated enhanced MR image shows 6.0 × 4.0 cm invasive ductal carcinoma including both exophytic nodular portion (*white arrow*) and central necrosis (*black arrow*).
**B,** Ultrasound tomography image obtained after steps 2–4 of fusion process highlights extent of mass margins similar to MRI, including both exophytic nodular portion (*white arrow*) and central necrosis (*black arrow*), assuming slight position differences between scanning in water (ultrasound tomography) and in air (MRI). Note dense parenchyma is displayed as semitransparent gray surrounding red tumor but is not obscuring tumor.

surrounding filamentous bands and connective tissue, as compared with the smooth margins of benign lesions, provides a potential means of predicting malignancy (Fig. 5).

Suspicious masses were primarily identified on DCE-MR images by their contrast enhancement. On fused ultrasound tomography images, suspicious masses were visualized as colorized regions that were above our currently specified threshold values of attenuation and sound speed. Color was needed in the fused image because gray-scale alone cannot display more than one quantified parameter. Color-coded thresholding of ultrasound tomography images therefore enhances the visibility of dense or stiff breast masses [30, 31, 34], which appear to correspond to suspicious masses on DCE-MRI (Fig. 6). Differentiation of malignant from parenchymal tissue was achieved without the use of contrast agents. These findings suggest that ultrasound tomography can effectively detect and characterize various breast lesions in a completely noninvasive manner even in women with dense breasts. This method can be used to isolate a suspicious lesion on ultrasound tomography images more consistently than on unenhanced MR images. Furthermore, this concordance provides justification for pursuing the ultrasound tomography method with the goal of leveraging its lower inherent cost (e.g., no large magnets, no shielding, and low cost of ultrasound transducers and electronics) and short examination times. Future studies utilizing microbubble-based contrast agents may provide additional differentiation capabilities and improve the diagnostic accuracy of ultrasound tomography images.

Of 55 masses reported from MRI examinations, 48 were found on ultrasound tomography. Ultrasound tomography examinations missed seven secondary masses that fell outside its scanning range (i.e., limited scanning range because of memory constraints of prototype used for study). The scanning range was occasionally limited for women with large breasts, for whom the scanning range had to be centered on the location of the known primary mass, because the storage memory of the initial ultrasound tomography prototype was 11 GB, which limited the number of slices that could be acquired. This limitation has now been removed: Memory is now 22 GB and will be improved further in future commercial versions. Despite this limitation, ultrasound tomography was able to detect an additional three masses that were not originally reported on standard ultrasound or mammography but were confirmed by MRI. These results warrant further study in our larger series of biopsy-proven masses being finalized for publication.

Several weaknesses and limitations arise from our described methods. Despite quantitative analysis, our results were based on subjective comparisons between MRI and ultrasound tomography. This method, however, is warranted given our goal to prospectively define initial ultrasound tomography thresholds based on MR appearances, thereby using MRI as the gold standard to validate the anatomic appearances of ultrasound tomography for both fibroglandular tissue distribution and tumor volumes. Information presented in this article is meant to become a baseline because our prototype is being prepared for large multicenter clinical trials. These trials will also facilitate further assessments of clinical relevance and specifications as a final commercial product is approached. Ultrasound tomography's ability to also detect and diagnose DCIS or intramammary lymph nodes is uncertain because they were not available for lesion analyses.

In summary, our pilot study has prospectively determined universal clinical threshold values that may be applied to ultrasound tomography images, thereby generating images showing overall breast anatomy and tumor conspicuity similar to DCE-MRI but without IV contrast material. As ultrasound tomography technology continues to mature in commercial versions, the absolute thresholds will be refined, but the overall concept of ultrasound tomography providing quantitative values for tissue discrimination appears secure. A strong concordance between ultrasound tomography–rendered and MRI-rendered breast anatomy was shown, indicating that ultrasound tomography could provide a lower-cost alternative to MRI for both diagnosis and automated volume–based assessments of breast characteristics, such as breast density [24, 25]. A forthcoming study of a larger cohort of biopsy patients will further address the diagnostic performance of ultrasound tomography.

## Acknowledgments

Special thanks to Olsi Rama, Lisa Bey-Knight, David Kunz, Erik West, and Amy Szczepanski for their contributions to this project.

## References

1. Lehman CD, Isaacs C, Schnall MD, et al. Cancer yield of mammography, MR, and US in high-risk women: prospective multi-institution breast cancer screening study. *Radiology* 2007; 244:381–388
2. Saslow D, Boetes C, Burke W, et al.; American Cancer Society Breast Cancer Advisory Group. American Cancer Society guidelines for breast screening with MRI as an adjunct to mammography. *CA Cancer J Clin* 2007; 57:75–89
3. Uematsu T, Yuen S, Kasami M, Uchida Y. Comparison of magnetic resonance imaging, multidetector row computed tomography, ultrasonography, and mammography for tumor extension of breast cancer. *Breast Cancer Res Treat* 2008; 112:461–474

4. Neubauer H, Li M, Kuehne-Heid R, Schneider A, Kaiser WA. High grade and non-high grade ductal carcinoma in situ on dynamic MR mammography: characteristic findings for signal increase and morphological pattern of enhancement. *Br J Radiol* 2003; 76:3–12
5. Onesti JK, Mangus BE, Helmer SD, Osland JS. Breast cancer tumor size: correlation between magnetic resonance imaging and pathology measurements. *Am J Surg* 2008; 196:844–850
6. Schnall MD. Application of magnetic resonance imaging to early detection of breast cancer. *Breast Cancer Res* 2001; 3:17–21
7. Warren RM, Pointon L, Thompson D, et al.; UK Magnetic Resonance Imaging in Breast Screening (MARIBS) Study Group. Reading protocol for dynamic contrast-enhanced MR images of the breast: sensitivity and specificity analysis. *Radiology* 2005; 236:779–788
8. Kuhl CK, Schild HH. Dynamic image interpretation of MRI of the breast. *J Magn Reson Imaging* 2000; 12:965–974
9. Bartella L, Smith CS, Dershaw DD, Liberman L. Imaging breast cancer. *Radiol Clin North Am* 2007; 45:45–67
10. Schnall MD. Breast MR imaging. *Radiol Clin North Am* 2003; 41:43–50
11. Chen W, Giger ML, Lan L, Bick U. Computerized interpretation of breast MRI: investigation of enhancement-variance dynamics. *Med Phys* 2004; 31:1076–1082
12. Chen W, Giger ML, Li H, Bick U, Newstead GM. Volumetric texture analysis of breast lesions on contrast-enhanced magnetic resonance images. *Magn Reson Med* 2007; 58:562–571
13. Wiener JI, Schilling KJ, Adami C, Obuchowski NA. Assessment of suspected breast cancer by MRI: a prospective clinical trial using a kinetic and morphologic analysis. *AJR* 2005; 184:878–886
14. Moore SG, Shenoy PJ, Fanucchi L, Tumeh JW, Flowers CR. Cost-effectiveness of MRI compared to mammography for breast cancer screening in a high risk population. *BMC Health Serv Res* 2009; 9:9
15. André MP, Janée HS, Martin PJ, Otto GP, Spivey BA, Palmer DA. High-speed data acquisition in a diffraction tomography system employing large-scale toroidal arrays. *Int J Imaging Syst Technol* 1997; 8:137–147
16. Johnson SA, Tracy ML. Inverse scattering solutions by a sinc basis, multiple source, moment method. Part I. Theory. *Ultrason Imaging* 1983; 5:361–375
17. Schreiman JS, Gisvold JJ, Greenleaf JF, Bahn RC. Ultrasound transmission computed tomography of the breast. *Radiology* 1984; 150:523–530
18. Natterer FA and Wubbeling F. A propagation-backpropagation method for ultrasound tomography. *Inverse Problems* 1995; 11:1225–1232
19. Liu DL, Waag RC. Propagation and backpropagation for ultrasonic wavefront design. *IEEE Trans Ultras Ferro and Freq Contr* 1997; 44:1–13
20. Ranger B, Littrup P, Duric N, et al. Breast imaging with acoustic tomography: a comparative study with MRI. (abstr) *Proc SPIE* 2009; 7265: 726,510
21. Duric N, Littrup P, Poulo L, et al. Detection of breast cancer with ultrasound tomography: first results with the computerized ultrasound risk evaluation (CURE) prototype. *Med Phys* 2007; 34:773–785
22. Duric N, Littrup P, Babkin A, et al. Development of ultrasound tomography for breast imaging: technical assessment. *Med Phys* 2005; 32:1375–1386
23. Li C, Duric N, Littrup P, Huang L. In vivo breast sound-speed imaging with ultrasound tomography. *Ultrasound Med Biol* 2009; 35:1615–1628
24. Glide-Hurst CK, Duric N, Littrup P. A new method for quantitative analysis of mammographic density. *Med Phys* 2007; 34:4491–4498
25. Glide-Hurst CK, Duric N, Littrup P. Volumetric breast density evaluation from ultrasound tomography images. *Med Phys* 2008; 35:3988–3997
26. Schmidt S, Duric N, Li C, Roy O, Huang Z. Modification of Kirchhoff migration with variable sound speed and attenuation for acoustic imaging of media and application to tomographic imaging of the breast. *Med Phys* 2011; 38:998–1007
27. Goss SA, Johnston RL, Dunn F. Comprehensive compilation of empirical ultrasonic properties of mammalian tissues. *J Acoust Soc Am* 1978; 64: 423–457
28. Duck FA. *Physical properties of tissue*. London, UK: Academic Press, 1990
29. Edmonds PD, Mortensen CL, Hill JR, et al. Ultrasound tissue characterization of breast biopsy specimens. *Ultrason Imaging* 1991; 13:162–185
30. Weiwad W, Heinig A, Goetz L, et al. Direct measurement of sound velocity in various specimens of breast tissue. *Invest Radiol* 2000; 35:721–726
31. Chang CH, Huang SW, Yang HC, Chou YH, Li PC. Reconstruction of ultrasonic sound velocity and attenuation coefficient using linear arrays: clinical assessment. *Ultrasound Med Biol* 2007; 33:1681–1687
32. ImageJ Website. http://rsbweb.nih.gov/ij/. Accessed August 2, 2009
33. D'Orsi CJ, Mendelson, EB, Ikeda DM, et al: *Breast Imaging Reporting and Data System: ACR BI-RADS—breast imaging atlas.* Reston, VA: American College of Radiology, 2003
34. Satake H, Nishio A, Ikeda M, et al. Predictive value for malignancy of suspicious breast masses of BI-RADS categories 4 and 5 using ultrasound elastography and MR diffusion-weighted imaging. *AJR* 2011; 196:202–209